ANNALS OF GEOPHYSICS, 61, 3, GD335, 2018; doi: 10.4401/ag-7591

“COMPARISON OF PALAEOSTRESS ANALYSIS, GEODETIC STRAIN RATES AND SEISMIC DATA IN THE WESTERN PART OF THE SULTANDAĞI FAULT IN TURKEY”

İbrahim Tiryakioğlu[1,2,*], Çağlar Özkaymak[2,3], Tamer Baybura[1], Hasan Sözbilir[4], Murat Uysal[1]

(1) Department of Geomatics, Faculty of Engineering, Afyon Kocatepe University, Afyonkarahisar, Turkey
(2) Earthquake Research and Implementation Center of Afyon Kocatepe University, Afyon, Turkey
(3) Department of Geology, Faculty of Engineering, Afyon Kocatepe University, Afyonkarahisar, Turkey
(4) Department of Geology, Faculty of Engineering, Dokuz Eylül University, İzmir, Turkey

Article history
Receveid November 21, 2017; accepted March 21, 2018.
Subject classification:
Crustal deformations; Measurements and monitoring; Satellite geodesy; Earthquake geology and paleostress analysis; Ground motion.

ABSTRACT

The Sultandağı Fault is an active dip-slip normal fault bounding the southeastern border of the NW-SE striking Afyon-Akşehir Graben, an actively growing rift area in western Anatolia. The historical and instrumental earthquake record suggest the existence of a large number of earthquakes that created surface ruptures in this system. The recent activities of the Sultandağı Faul twere evidenced bytwo earthquakes that occurred on February 3, 2002 (Mw=6.3 and Mw=6.0) and caused a surface rupture up to 26 km along with an approximately 30 cm vertical displacement. The possible continuation of this earthquake migration towards the west, seismic gaps existing in the region, the presence of historical destructive earthquakes, and the active faults reveal the seismic hazard around the province of Afyonkarahisar. In this study, we determined the fault activities and stress directions in the western part of the Sultandağı Fault by comparing the results from the Palaeostress analysis of fault segments, focal mechanism solutions of recent earthquakes and geodetic analysis. The geologic, geodetic and earthquake data all indicate that both northern and southern master faults of the middle part of the Afyon-Akşehir Graben are dip-slip normal faults and were shaped under a NW-SE and NE-SW-directed bimodal extensional tectonic regime during the Quaternary-Holocenethe period.

1. INTRODUCTION

The Afyon-Akşehir Graben (AAG), approximately 4-20 km wide and 130 km long, NW-SE striking, is defined as an actively growing rift area and constitutes the southeastern part of the Akşehir-Simav Fault System (ASFS), which is one of the most significant seismogenic zones in the West Anatolian Extensional Province (Figure 1) [Koçyiğit, 1984; Koçyiğit et al., 2000; Koçyiğit and Özacar, 2003]. The historical and instrumental earthquake records suggest the existence of many destructive earthquakes that created surface ruptures in AAG. The last surface-rupturing earthquakes (Mw=6.3 and Mw=6.0) occurred on February 3, 2002 along the Sultandağı Fault, which controls the southeastern margin of AAG. The total surface rupture that developed during these earthquakes was approximately 26 km with the maximum vertical displacement being 30 cm [Emre et al., 2003; Akyüz et al., 2006]. In the literature, these earthquakes are considered to be part of seismic migration advancing in the NW direction on the Sultandağı Fault and influenced by the earthquakes in the east of AAG particularly the Doğanhisar-Ilgın earthquake that occurred in 1921, followed by the Argıthanlı earthquake in 1946, and the Sultandağı earthquake in 2000 [Demirtaş et al., 2002; Emre et al., 2003] (Figure 1).

There are only limited number of studies on the ac-

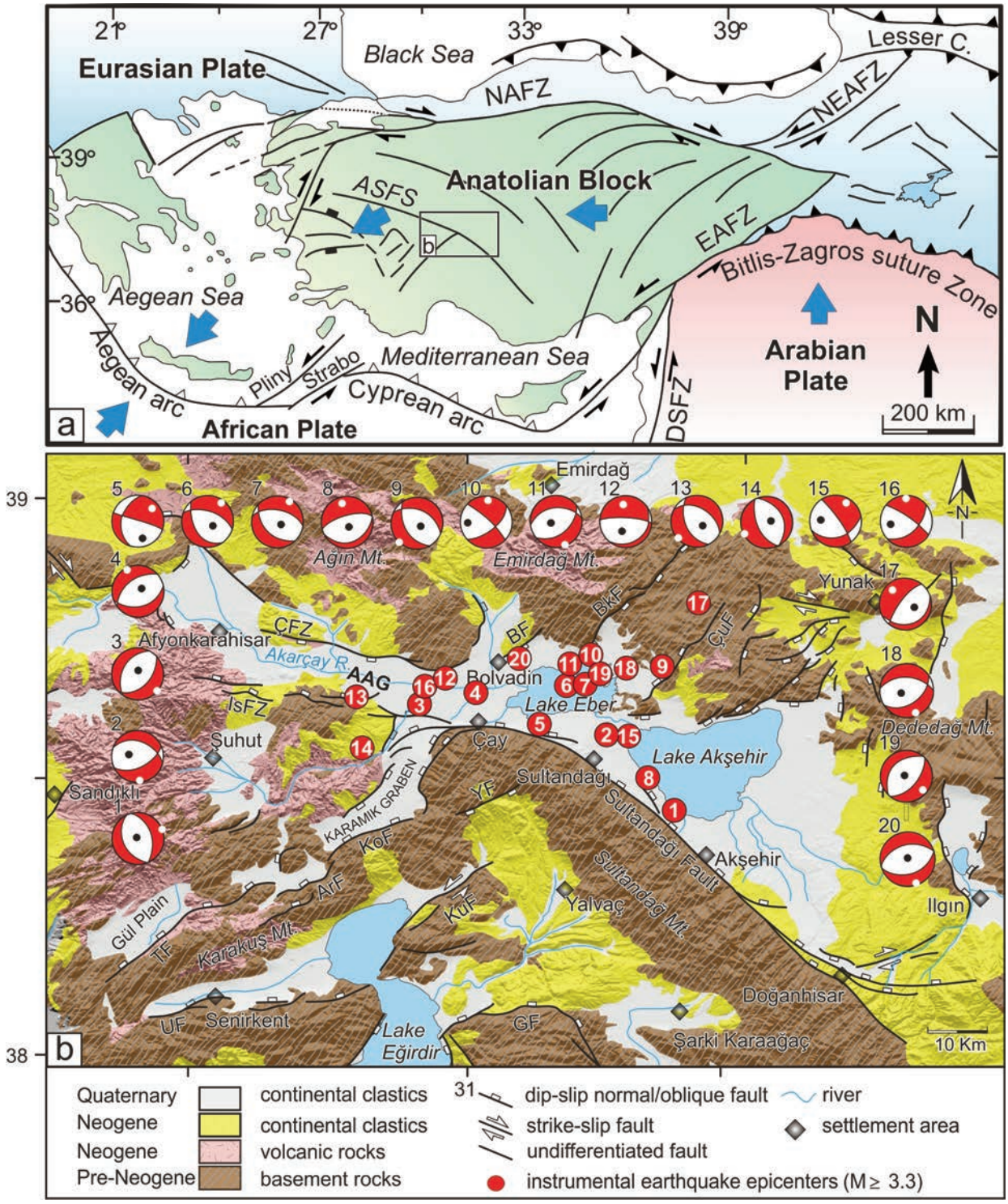

FIGURE 1. a) Tectonic outline of the eastern Mediterranean area (compiled from Kaymakcı, 2006 and Özkaymak, 2015). Abbreviations: ASFS, Aksehir Simav Fault System; DSFZ, Dead Sea Fault Zone; EAFZ, East Anatolian Fault Zone; NAFZ, North Anatolian Fault Zone; NEAFZ, Northeast Anatolian Fault Zone. b)The geology map of AAG and its immediate vicinity (issued from Turan, 2002, Emre et al., 2011, Tiryakioglu et al., 2015, Özkaymak et al., 2017] showing the epicenter distributions and the results of the focal mechanism of some of the earthquakes that occurred during the instrumental period. Abbreviations: ÇFZ: Çobanlar Fault Zone; IsFZ: Işıklar Fault Zone; BF: Bolvadin Fault; BkF: Büyük Karabağ Fault; ÇuF; Çukurcak Fault; YF: Yarıkkaya Fault; KuF: Kumdanlı Fault; GF: Gelendost Fault; KoF: Kocbeyli Fault; ArF: Arızlı Fault; UF: Uluborlu Fault; TF: Tatarlı Fault.

tive tectonics of AAG with most examining the period after the 2002 Çay earthquakes [Demirtaş et al., 2002; Emre et al., 2003; Koçyiğit and Ozacar., 2003; Ozden et al., 2002; Yürür et al., 2003; Ulusay et al., 2004; Akyüz

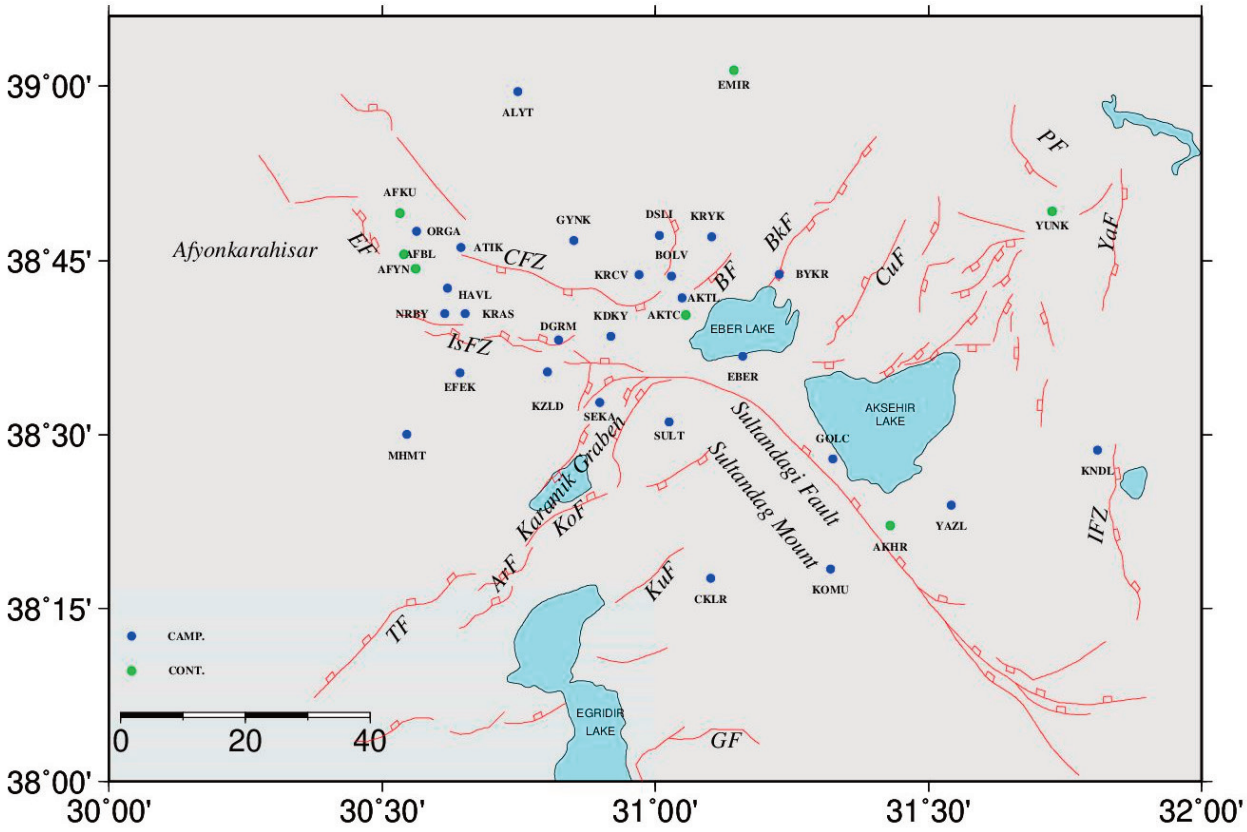

FIGURE 2. Tectonic GNSS Network.

et al., 2006, Aktuğ et al. 2010]. In these studies, the main focus is on the kinematic properties and geometry of the active tectonic structures and the seismic source of the 2002 Çay earthquakes in AAG. However, it is still not clear whether the NW-migrating earthquake failures that started in 1921 during the instrumental period on the Sultandağı Fault will move in the NW direction in future. The first palaeoseismological study on the active Sultandağı Fault in AAG was conducted by Akyüz et al. [2006], who reported two events with similar dip-slip properties to the 2002 Çay earthquake; one in the Maltepe trench after AD 1150 and the other in the Çay trench before AD 760. The authors stated that parts of the Sultandağı Fault had not ruptured in the instrumental period. Therefore, they suggested that moderate-sized earthquakes could be expected in future. However, other studies indicate that there is a seismic gap around Afyonkarahisar province located in the northwestern part of AAG [Demirtaş et al., 2002; Koçyiğit et al., 2002; Emre et al., 2003]. These controversial reports reveal the importance of undertaking further active tectonic studies in the western part of AAG within the regional tectonic framework of western Anatolia.

The first comprehensive study in the region was conducted by Aktuğ et al. in 2009, who used GNSS observations to determine the extent of deformation created by the 2002 earthquakes. In the present study, we aimed to examine the velocity field of the current plate in the western part of the Sultandağı Fault. To this end, GNSS data of the fault was collected to determine the extent and directions of the strain in the region. Furthermore, the palaeostress field orientations of the active faults in AAG were used to create a kinematic framework of faulting that developed in AAG during the Pliocene-Quaternary period.

2. GNSS OBSERVATIONS AND STRAIN ANALYSIS

A GNSS network has been established to performed strain analysis in the region. The GNSS network contains a total of 27 sites, of which 19 are campaign-type ground sites and the remaining 9 are Continuously Operating Reference Stations (CORS) (Figure 2).

In this study, the GNSS network was surveyed during three GNSS campaigns that took place between October 2012 and October 2015. All the GNSS measurements were collected simultaneously with minimum 8 hours data per day at a sampling rate of 15 seconds. In this project, receivers which can record GNSS data were used (Table 1).

Using the given parameters, the GNSS observations were collected on the network with Ashtech and Thales

Instrument	Number	Firm
Geodetic GNSS Rec	7	Ashtech Z-Xtreme with Geodetic Antenna IV
Geodetic GNSS Rec	3	Thales Z-Max and Antenna

TABLE 1. GNSS Equipment.

GNSS receivers A ground monument (SULT site) and a pillar (NRBY Site) facilitated by the network are shown in Figure 3.

The collected GNSS data was processed using the satellite orbits, atmospheric zenith delays, and earth rotation parameters using carrier phase measurements and pseudo-range observations. GLOBK utilizes a KALMAN filter to estimate the velocity of the measurement sites [Herring et al. 2010]. During the analysis, L3, the ionosphere-independent linear combination of the L1 and L2 carrier waves, was used. The FES2004 OTL grid allowed interpolating the Ocean Tide Loading (OTL) components from a global grid [Lyard et al. 2006; Herring et al. 2010; Ozener et al. 2012, Tiryakioglu, 2015]. Data from all measurements was processed using the Eurasia-Fixed International Terrestrial Reference Frame (ITRF08_EURA).

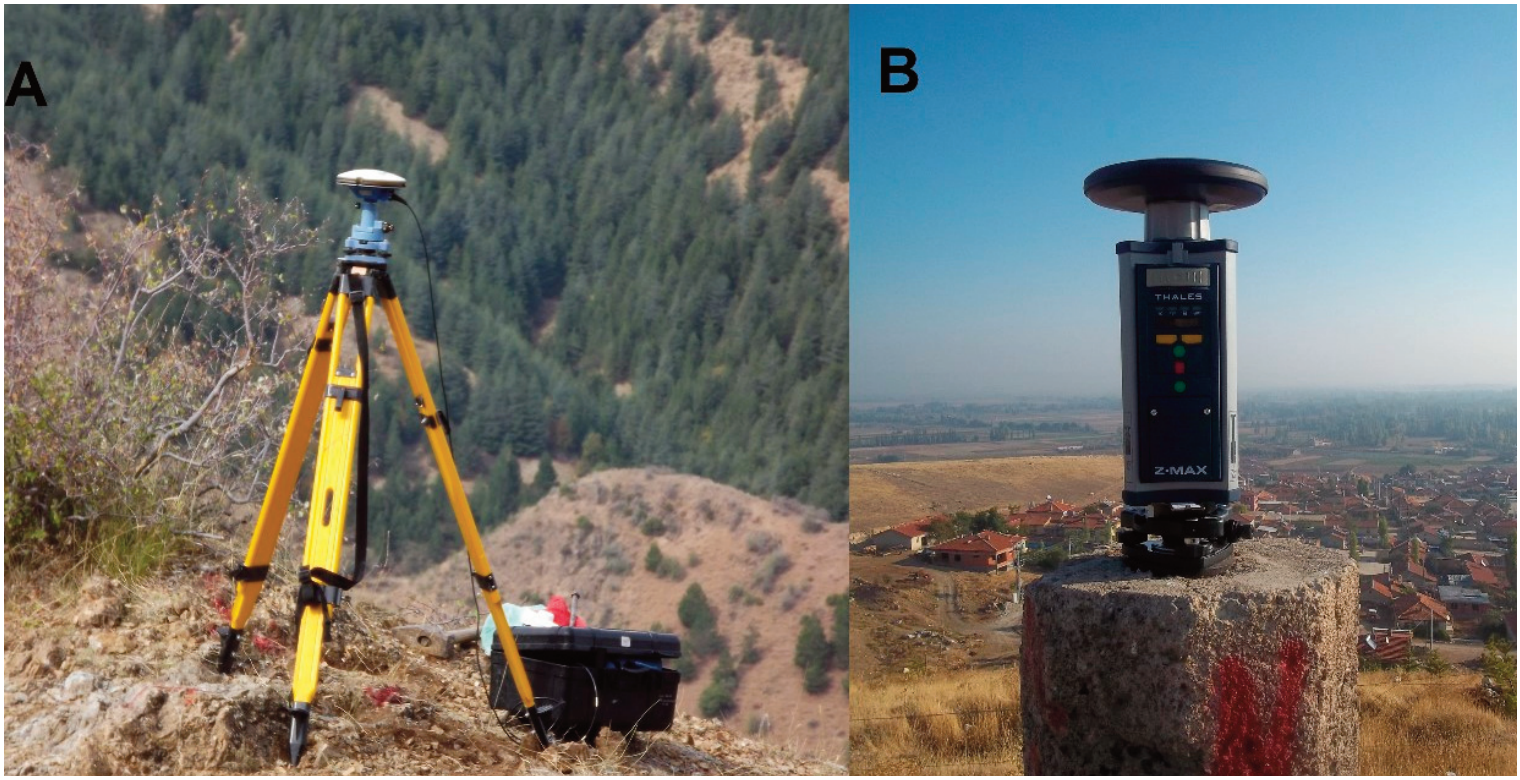

FIGURE 3. Ground monument (A-SULT Site), pillar (B-NRBY Site)

Station	City/Country	Station	City/Country
MATE	Matera, Italy	ZECK	Zelenchukskaya, Russia
NICO	Nicosia, Cyprus	SOFI	Sofia, Bulgaria
NSSP	Yerevan, Armenia	ISTA	Istanbul, Turkey
MERS	Mersin, Turkey	GLSV	Kiev, Ukraine
CRAO	Simeiz, Ukraine	RAMO	Mitzpe Ramon, Israel
TEHN	Tahran, Iran	BUCU	Bucharest, Romania
ANKR	Ankara, Turkey	TELA	Tel Aviv, Israel

TABLE 2. IGS stations used in analysis.

GAMIT (GPS Analysis))/GLOBK (GLOBal Kalman) software developed by Massachusetts Institute of Technology. The GAMIT module can estimate 3D coordinates,

The horizontal velocity components were estimated according to the ITRF EURA fixed frames using a set of 14 International GNSS Service (IGS) sites. Table 2 lists

Site	Lat (°)	Lon (°)	V_E (mm/yr)	V_N (mm/yr)	Se (mm/yr)	Sn (mm/yr)	First Epoch	Last Epoch	Interval (Year)	Number of obs.
AFBL	30.540	38.759	-21.33	-3.80	0.35	0.37	2012.52	2016.37	3.85	Cont.
AFKU	30.533	38.818	-19.97	-2.02	0.46	0.50	2012.52	2016.37	3.85	Cont.
AFYN	30.561	38.738	-19.91	-4.26	0.33	0.36	2008.75	2016.37	7.62	Cont.
AKHR	31.430	38.369	-20.43	-4.20	0.28	0.30	2008.75	2016.37	7.62	Cont.
AKTL	31.049	38.697	-19.24	-3.03	0.93	1.08	2012.77	2016.37	3.6	4
ATIK	30.644	38.769	-21.21	-1.43	1.07	1.06	2012.77	2016.37	3.6	4
BOLV	31.029	38.728	-20.53	-0.93	0.63	0.73	2012.77	2016.37	3.6	5
BYKR	31.227	38.731	-24.37	-9.63	0.63	0.72	2012.77	2016.37	3.6	3
DGRM	30.823	38.636	-18.61	-3.96	0.98	1.19	2012.77	2016.37	3.6	4
DSLI	31.008	38.787	-19.43	-4.31	0.80	0.95	2012.77	2016.37	3.6	4
EBER	31.160	38.613	-17.54	-2.93	0.72	0.84	2012.77	2016.37	3.6	5
EFEK	30.642	38.589	-21.31	-2.74	0.56	0.63	2012.77	2016.37	3.6	4
EMIR	31.144	39.022	-20.64	-2.47	0.28	0.31	2008.75	2016.37	7.62	Cont.
GYNK	30.851	38.779	-19.97	-4.19	0.81	0.99	2012.77	2016.37	3.6	4
HOYK	30.620	38.711	-23.89	-1.73	0.16	0.20	2006.57	2016.37	3.6	6
HVAL	31.035	38.693	-19.90	-4.43	0.61	0.68	2012.77	2016.37	3.6	4
KDKY	30.919	38.642	-21.22	-4.03	0.77	0.90	2012.77	2016.37	3.6	4
KRAS	30.652	38.674	-17.08	-3.62	0.79	0.92	2012.77	2016.37	3.6	4
KRCV	30.970	38.730	-18.15	-3.49	0.76	0.91	2012.77	2016.37	3.6	5
KRYK	31.104	38.784	-20.32	-4.68	0.86	1.02	2012.77	2016.37	3.6	4
KZLD	30.803	38.591	-20.87	-2.75	0.99	1.10	2012.77	2016.37	3.6	3
NRBY	30.546	38.501	-20.23	-6.48	0.76	0.90	2012.77	2016.37	3.6	4
ORGA	30.615	38.674	-19.76	-3.93	0.62	0.70	2012.77	2016.37	3.6	4
SEKA	30.563	38.792	-21.79	-2.87	0.67	0.77	2012.77	2016.37	3.6	4
SHUT	30.898	38.547	-18.86	-4.66	0.26	0.31	2008.72	2013.67	4.95	6
SULT	31.026	38.519	-30.17	-2.99	0.98	1.10	2012.77	2016.37	3.6	3
YUNA	31.726	38.820	-19.41	-2.45	0.28	0.31	2008.75	2016.37	7.62	Cont.

TABLE 3. Site name, period of observation and Horizontal velocities and corresponding 1σ errors in the Eurasia Fixed Reference Frame.

the names of the IGS stations used in the analysis.

Suitable IGS stations were investigated to use in the GAMIT module for the Global stabilization procedure. In this stage, the IGS stations that provided the best re-

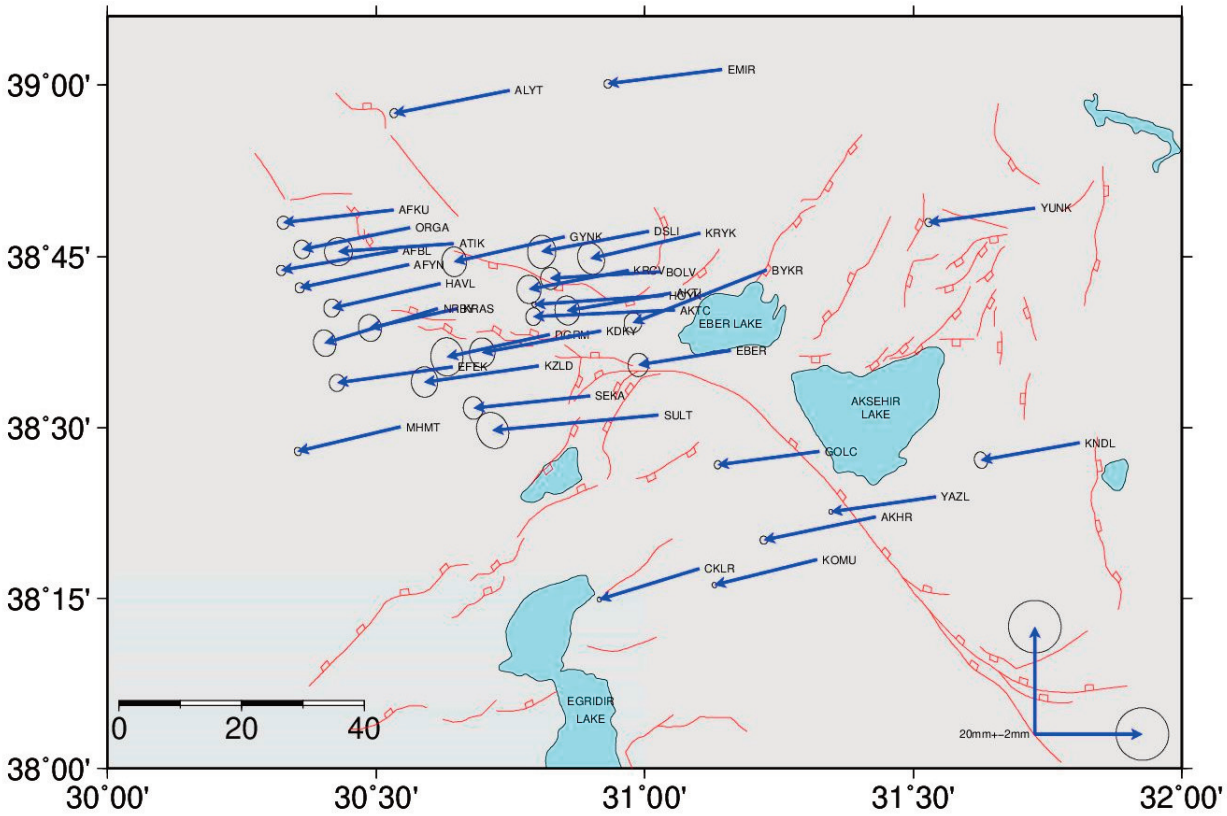

FIGURE 4. Velocities and their uncertainties with respect to the Eurasia-fixed reference frame.

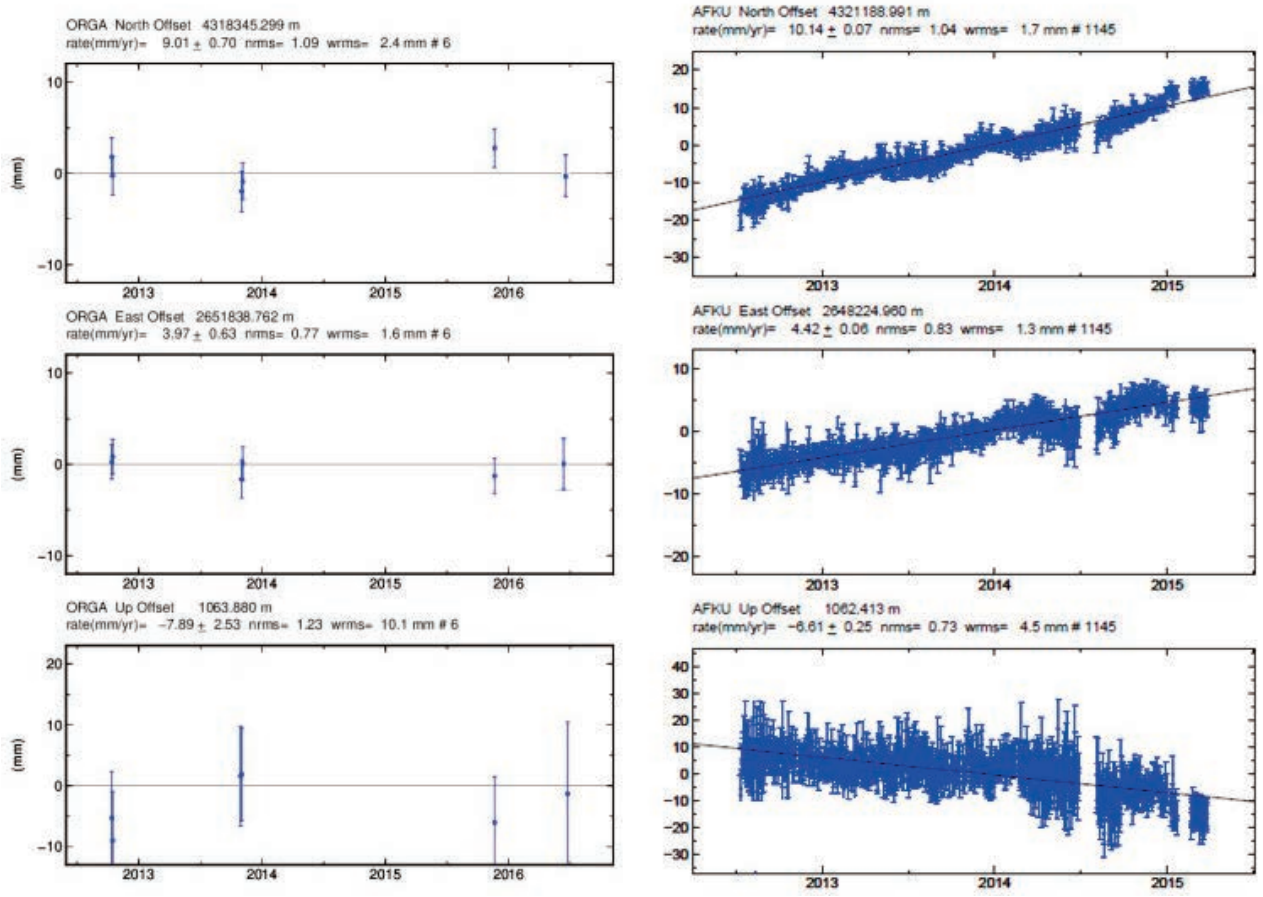

FIGURE 5. Time series of the ORGA(left) and AFKU (right) stations.

sults after producing four iterative solutions were selected as the stabilization stations. The precise coordinates were obtained using a trend analysis of the time-series in the KALMAN filtering technique of the GLOBK program to ensure stabilization for the determination of the velocity vectors of the stations. The post root mean square (RMS) values of velocity calculated after GLOBK stabilization were obtained as 0.4 mm/yr for the Eurasian plate under 1 mm/yr. At the end of assessments, the Eurasian plate was accepted as stable and the velocity values obtained are given in Table 3 and Figure 4. Figure 5 show ITRF 2005 time-series of positions for two stations Continously and Campaing, namely AFKU and ORGA (Table 3).

A strain analysis was conducted with the geodsuit software package using the current velocity field of the region [GeodSuit 2017].

The relationship between the velocities and strain parameters obtained by GNSS measurements can be written as:

$$u = Lx + \dot{t} \tag{1}$$

Where, $\boldsymbol{u}$: the site velocities, $\dot{t}$: translational velocities, $\boldsymbol{x}$: position vector, and L: the deformation tensor due to the annual variation of the strain parameters ($\dot{e}$) and the solid block rotations ($\dot{w}$). L tensor can be written as (Feigl, 1990);

$$L = \dot{e} + \dot{\omega} \tag{2}$$

The relationship between the $\dot{w}$ and $\dot{e}$ and strain parameters can be written as (Turcotte and Schubert, 1982);

$$\dot{\omega}_{ij} = \frac{1}{2}\left(\frac{\partial u_i}{\partial x_j} - \frac{\partial u_j}{\partial x_i}\right),\ i \neq j,\ \dot{\omega}_{ii} = 0,\ i = j \tag{3}$$

$$\dot{e}_{ij} = \frac{1}{2}\left(\frac{\partial u_i}{\partial x_j} + \frac{\partial u_j}{\partial x_i}\right) \tag{4}$$

Wherein the partial derivatives correspond to those gradients that north and east directions. A covariance weighted method has been used to obtain the strain rates from the GNSS velocities (Shen et al., 1996). In this method, the effect of the surrounding GNSS velocities in calculating the strain velocities at any point can be modelled as follows;

$$C_{ij} = Q_{ij} \exp \frac{\left\|\dot{r}_x\right\|^2 + \left\|\dot{r}_y\right\|^2}{\sigma_D^2} \tag{5}$$

where Qij covariance matrix of used velocities, are the position vectors to the x and y coordinates of the GNSS points. σ_d is the smoothing factor used for positional smoothing such that when σ_d is taken as 50 km, then the contribution of a point located at a distance of 25 km is around 80%. In the calculations, considering the density of the network σ_d is taken 50 km as a priori and is iteratively updated at each grid point based on the resolution of the reweighted data set following (Shen et al., 1996).

In this study, a two-dimensional strain analysis was performed due to the lack of desired accuracy for a three-dimensional analysis using the GNSS technology. The study area was divided into a 5x5 km grid and strain fields were determined for each grid. The stations that had data from two campaign times were excluded from further analysis. The resulting strain field is presented in Figure 6.

3. KINEMATIC ANALYSIS

The faults controlling the northern and southern margins of AAG mainly represent the structural contact between pre-Quaternary basement rocks and modern basin fills (Figure 1b). The middle part of AAG consists of many WNW-ESE-striking parallel/sub-parallel dip slip normal fault segments with a typical maximum length in the range of 5-15 km. One of the northern bounding fault zones is the Çobanlar Fault Zone (ÇFZ), which extends approximately 30 km and strikes in the WNW-ESE direction between Afyonkarahisar and Bolvadin (Figure 1b, Figure 7a). On the opposite side of ÇFZ, the southern margin of AAG is represented by the Işıklar Fault Zone extending approximately 15 km in the WNW-ESE between Afyonkarahisar and Çay. Numerous north-dipping quasi-parallel normal fault segments form a step-like geometry (Figure 7b). In the SW of Çay, many NE-SW-striking dip-slip normal faults form the Karamık Quaternary Graben, which extends in a direction perpendicular to AAG. The southeastern margin faults exhibit prominent Quaternary fault scarps and represent the structural contact between pre-Neogene basement rocks and modern graben fill. The northwestern side has a relatively gentle morphology but the boundary fault can easily be followed between Neogene clastics and modern graben fill (Figure 1b). The main southern boundary fault is represented by 100 km long Sultandağı Fault. The footwall of the fault, Sultandağı High, has the highest peak (2.675 m) in Middle-Western Anatolia and is represented by pre-Neogenie metamorphic rocks mainly consisting of phyllites and

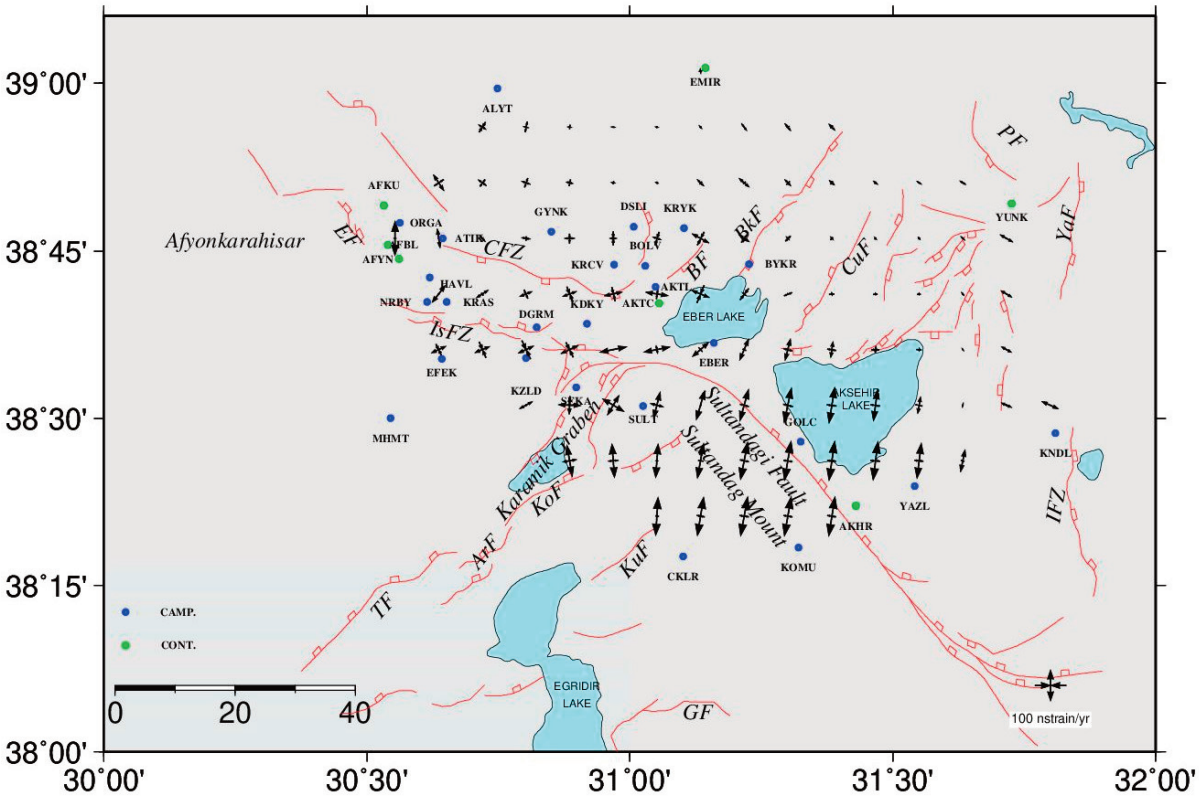

FIGURE 6. Strain field in the study area. The red lines indicate the active faults.

FIGURE 7. (a) A field view of the Çobanlar Fault Zone (CFZ), (b) A field view of the Işıklar Fault Zone (IsFZ) showing a step-like geometry. (c) A field view of the Çukurcak Fault (CuF), (d) A close image of the CuF plane demonstrating slickensides (e) A field view of the Bolvadin Fault (BF) (f) A close image of the BF plane demonstrating slickensides.

schists. Along the mountain front, well-developed alluvial fans, triangular facets and v-shaped drainage basins indicate that the Sultandağı mountain front is tectonically active. Many north dipping fault surfaces exhibit well-preserved striation and fault-related structures along the mountain front. The opposite side of the graben is controlled by several NE-SW-trending normal fault segments such as Bolvadin, Büyük Karabağ and Çukurcak Faults (Figure 1b, Figures 7c,d,e and f).

4. FAULT-SLIP DATA

The stress field orientations of master faults bounding the middle part of AAG were evaluated in terms of kinematics and the stress history of the region. The structural relationships between striations and fault-plane related structures were used for the assessment of age relations and sense of motion. The fault-slip data were analyzed using the stress inversion method developed by Angelier [1984, 1991, 1994] and computed with the software by Hardcastle and Hills [1991]. At Station A (middle part of ÇFZ), the stress analysis of the fault-slip measurement shows an approximately vertical σ1 axis plunging at 72° whereas the σ2 and σ3 axes were almost horizontal plunging at 14° and 11°, respectively (Figure 8 and Table 4). Similarly, the striation set on the eastern slip surfaces of ÇFZ (at Station B) displayed σ2 and σ3 orientations of 280°/14° and 159°/03° (trend/plunge), respectively, with an almost vertical σ1 axis plunging at 74° and trending at 123° (Figure 8 and Table 4). The results suggest that dip-slip normal faulting is consistent with an approximately NNW-SSE and NNE-SSW-trending extensional stress regime. The kinematic data collected from the eastern branches of IsFZ (Station C) yielded a nearly vertical σ1 axis (83°) trending 271° whereas the σ2 and σ3 axes have the attitudes of 069°/06° and 159°/03°, respectively (Figure 8 and Table 4). This suggests the existence of a NW–SE extension.

Station D was located on the southeastern margin of the Karamık Graben (Figure 8). The results of the fault slip measurements at Station D demonstrate a relatively steeply plunging σ1 axis (72°) but sub-horizontal σ3 axes (18°), and the orientation of the σ2 axis was 017°/04°. The fault slip measurements from the Karamık Graben were consistent with a NW-SE extensional tectonic regime.

We used kinematic data from the Sultandağı Fault at two stations (E and F, Table 4, Figure 8). The orientations of the computed principal stresses were as follows: σ1 is almost vertical at both stations (78° and 84°, respectively) while σ2 and σ3 were sub-horizontal (Table 4). The stress trajectories orientations along the fault suggest an approximately NNE-SSW and NE-SW-directed extension.

The fault slip data collected from Station G along the Bolvadin Fault included a nearly vertical σ1 axis (81°) whereas the σ2 and σ3 axes have the attitudes of 240°/03° and 149°/09°, respectively. The results show that Bolvadin Fault is a nearly pure dip-slip normal fault and the extension at Station G is oriented in the NW-SE direction (Figure 8 and Table 4). At Station H located on the NE-SW-striking Çukurca Fault, the inverse stress analysis of the fault slip measurement show an approximately vertical σ1 axis plunging at 83° and almost horizontal σ2 and σ3 plunging at 02° and 07°, respectively. This result indicates an approximately NW-SE extension on the Çukurcak Fault.

No	Fault	Number of slip data	1	2	3		Max ANG
A	Çobanlar Fault Zone	09	124/72	264/14	357/11	0.511	13
B	Çobanlar Fault Zone	08	123/74	280/14	011/06	0.150	20
C	Işıklar Fault Zone	13	271/83	069/06	159/03	0.171	19
D	Karamık Graben	10	121/72	017/04	286/18	0.028	12
E	Sultandağı Fault	10	251/84	103/05	012/03	0.615	09
F	Sultandağı Fault	09	192/78	311/06	043/11	0.130	09
G	Bolvadin Fault	10	351/81	240/03	149/09	0.380	05
H	Çukurcak Fault	10	012/83	267/02	177/07	0.456	05

TABLE 4. Results of the Palaeostress analysis on the measurements of slickensides in the study area (see Figure 8 for locations). Abbreviations: Max ANG: Maximum misfit angle

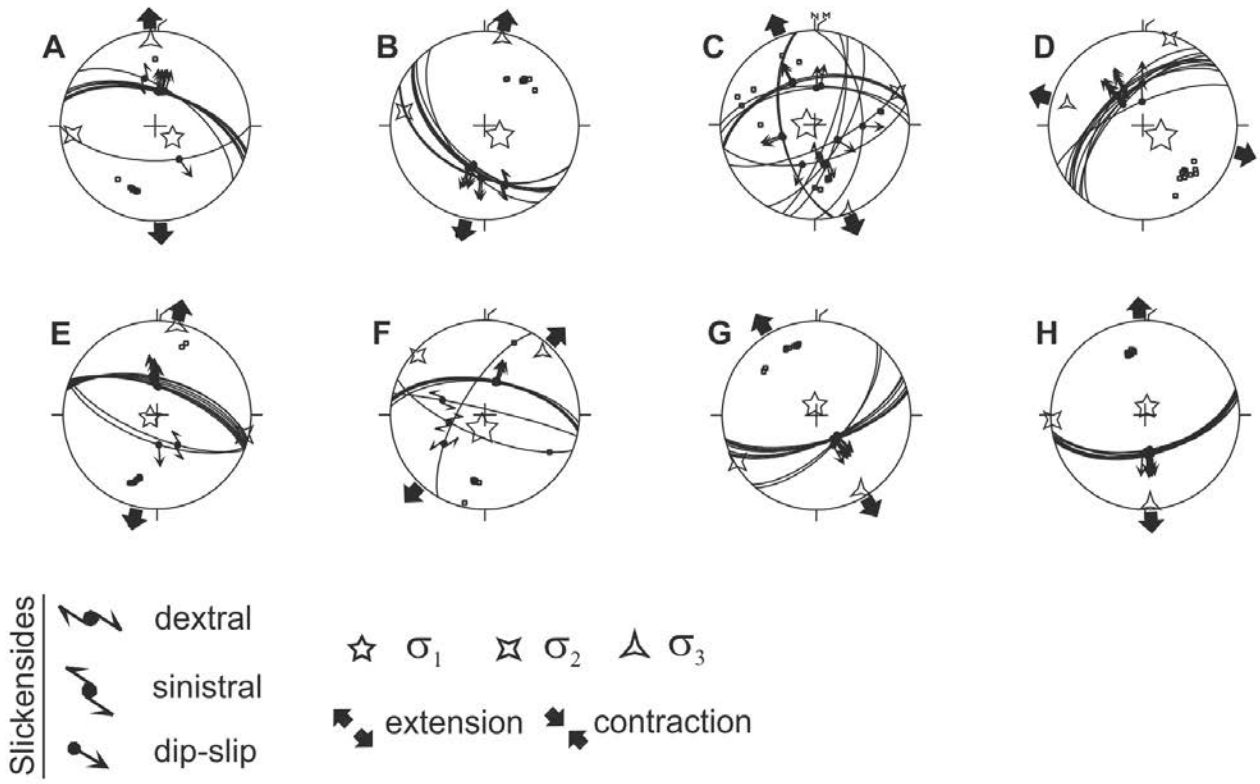

FIGURE 8. (a) Palaeostress analysis performed on the studied faults by using of the sofware Angelier [1984, 1991, 1994] and Hardcastle and Hills [1991]. The equal-area lower-hemisphere stereoplots illustrate the fault-slip surface, slip direction and principal stress axis orientations data and the position of principal stress axes. Large circles are the fault surfaces and the arrows are striations (see Table 4 for details and Figure 9 for locations).

5. EARTHQUAKE DATA

For the instrumental period, five focal mechanism solutions of moderate size and destructive earthquakes have been reported along the Sultandağı Fault and the surrounding area (Table 5, Figure 1b). The focal mechanism solution of the 2000 Sultandağı earthquake (Mw=6.0) indicates the existence of a NE-SW on the Sultandağı Fault (1, Table 5, Figure 1b). The data from the 2002 Çay (Mw=6.3), 2009 Ortakarabağ (Mw=3.8) and 2016 Bolvadin (Mw=3.8) earthquakes shows that the recent activities along AAG are related with a NW-SE-directed almost pure extension (2, 18 and 20 in Table 5, Figure 1b) while the focal mechanism solution of the 2002 Çay earthquake (Mw=6.0) suggests an approximately WNW-ESE-directed extension (3 in Table 5, Figure 1b).

6. DISCUSSION AND CONCLUSION

Based on the obtained velocity field shown in Figure 4, it was found that the study area moves towards west at an average annual velocity of 20 mm respect to the Eurasian reference system. These results are in agreement with those of other studies conducted in the region. The strain fields were determined using the velocities obtained from the assessment of GNSS observations. These strain fields indicated the dominance of a N-S extension regime of the western part of the region. The strain values in the western part of the region were at a maximum level while those in the eastern part were found to be very low.

There was a slight strain in the form of a NW-SE extension in the west part of the region. It was interesting to determine small strain values particularly in the Bolvadin region. It is considered that this strain was formed by the earthquakes of a 6.3 magnitude that occurred around Bolvadin in 2002. This is supported by several studies that have reported that the 2002 earthquakes caused an energy transfer towards west [Demirtaş et al. 2002; Koçyiğit et al. 2002; Yürür et al., 2003; Ergin et al. 2009] as demonstrated in the results of the strain analysis.

Palaeostress analysis were conducted on the boundary faults of the middle part of AAG to determine the stress directions on the faults during the neotectonic period. The fault-slip data indicate that both northern and southern master faults of AAG are dip-slip normal faults and were shaped under a NW-SE and NE-SW bimodal extensional tectonic regime during the Quater-

No	Date	Location	Mag. (Mw)	Depth (km)	Coordinate Lat.(N)-Long.(E)	Direction of Extension	References
1	15.12.2000	Sultandağı	6.0	5.8	38.59-31.16	NE-SW	1,3,4,5,7,8
2	03.02.2002	Çay	6.3	10.0	38.58-31.25	NW-SE	1,3,4,5,8
3	03.02.2002	Kadıköy	6.0	10.0	38.69-30.84	NW-SE	1,3,4,5,8
4	03.02.2002	Kadıköy	4.6	10.0	38.64-31.00	NW-SE	8
5	13.05.2002	Eber	4.3	8.7	38.59-31.12	NE-SW	8
6	26.06.2002	Eber Gölü	4.2	17.7	38.66-31.18	NE-SW	8
7	05.08.2002	Derekarabağ	4.3	10.0	38.68-31.20	NE-SW	8
8	03.07.2004	Dereçine	4.5	13.0	38.50-31.33	NW-SE	8
9	08.08.2004	Çukurcak	3.8	7.5	38.70-31.35	NE-SW	8
10	07.09.2004	Derekarabağ	4.5	10.0	38.69-31.20	NE-SW	8
11	16.09.2004	Derekarabağ	4.3	10.0	38.69-31.19	NW-SE	8
12	08.11.2004	Kadıköy	4.2	16.0	38.67-30.92	N-S	8
13	15.05.2005	Değirmendere	4.2	11.3	38.61-30.78	NE-SW	8
14	08.11.2006	Kızıldağ	3.3	12.0	38.55-30.79	NE-SW	8
15	19.04.2007	Taşköprü	4.0	18.1	38.57-31.25	NE-SW	8
16	06.05.2007	Kadıköy	3.3	18.5	38.66-30.86	NE-SW	8
17	18.01.2009	Eydemir	3.5	15.0	38.81-31.40	NW-SE	8
18	15.09.2009	Ortakarabağ	3.8	2.00	38.70-31.27	NW-SE	1, 6
19	21.12.2009	Derekarabağ	3.7	14.8	38.68-31.21	NW-SE	8
20	18.10.2016	Bolvadin	3.8	9.00	38.69-31.06	NW-SE	2, 6

TABLE 5. Results of the focal mechanism solutions of earthquakes that occurred in AAG (see Figure 1b for locations). References: 1) EMSC, (2016) 2) Pınar, (2016), 3) Erdik et al., (2002), 4) USGS, (2016), 5) Tan et al., (2008), 6) KANDILLI, (2016), 7) Taymaz and Tan., (2001), 8. Kalafat and Görgün, 2017

nary period. The bimodal extension in AAG is also evidenced by the focal mechanism solutions of the recent earthquakes in the region. The stress direction data of the palaeostress analysis, focal mechanism solutions of recent earthquakes and GNSS analysis related to the Sultandağı Fault are almost consistent. Similar to the results of the analysis on the 2000 Sultandağı earthquake (M_W: 6.0) (1 in Figure 9 and Table 5) indicating a NE-SW-directed extensional tectonic regime in the south of Lake Akşehir, the palaeostress analysis of the Sultandağı Fault around Çay (E and F, Figures 8,9 and Table 4) suggest NW-SE trending normal faulting consistent with a NE-SW extensional stress regime. According to the GNSS analysis, in the same region, the stress was also in the NE-SW direction (Figure 9). Similar extension directions are also obtained from the analysis of recent earthquakes with magnitudes of 3.3 to 4.2 in the last decades occurred in the hanging wall of the Sultandağı Fault (e.g. 6,7, 13,14, Figure 9). Besides this, results of focal mechanism solutions of some recent earthquakes occurred in the middle part of the AAG, (e.g. 5, 10, 15, 16) show that some recent earthquakes predominantly have strike-slip mechanisms. Strike-slip deformation in rift basins may develop in transfer faults constituting linkage between two adjacent crustal sectors undergoing differential extension (e.g. Gibbs, 1990; Peacock et al., 2000; Acocella et al., 2005). This type of local contractional strains are also seen in GNSS strain analysis (Figure 9) and probably be associated with the occurrence of transfer faults linking to NE-SW and NW-SE-striking normal faults in the middle part of the AAG. This possibility should be carried out in further works in the region. The results of the inverse analysis of the fault-slip measurements along the Bolvadin and Çukurca faults revealed a steeply plunging σ3 axis and a NW-SE extension (G and H, Figures 8,9 and Table 4) during the 2016 Bolvadin (20 in Figure 9 and Table 5), 2009 Eydemir, Ortakarabağ and Derekarabağ (17,18 and 19 in Figure 9 and Table 5) 2004 Derekarabağ (20 in Figure 9 and Table 5) earthquakes. The NW-SE-directed extensional active tectonic regime around the Bolvadin and Eber areas are also evidenced by the results of the GNSS analysis in the present study. The palaeostress analysis along the NE-SW striking boundary faults of the Karamık Graben and the focal mechanism solution of the 2002 Çay Earthquake (Mw=6.0) indicate the existence of a NW-SE extensional stress (3 and D in Figure 9). However, the GNSS calculations for this region indi-

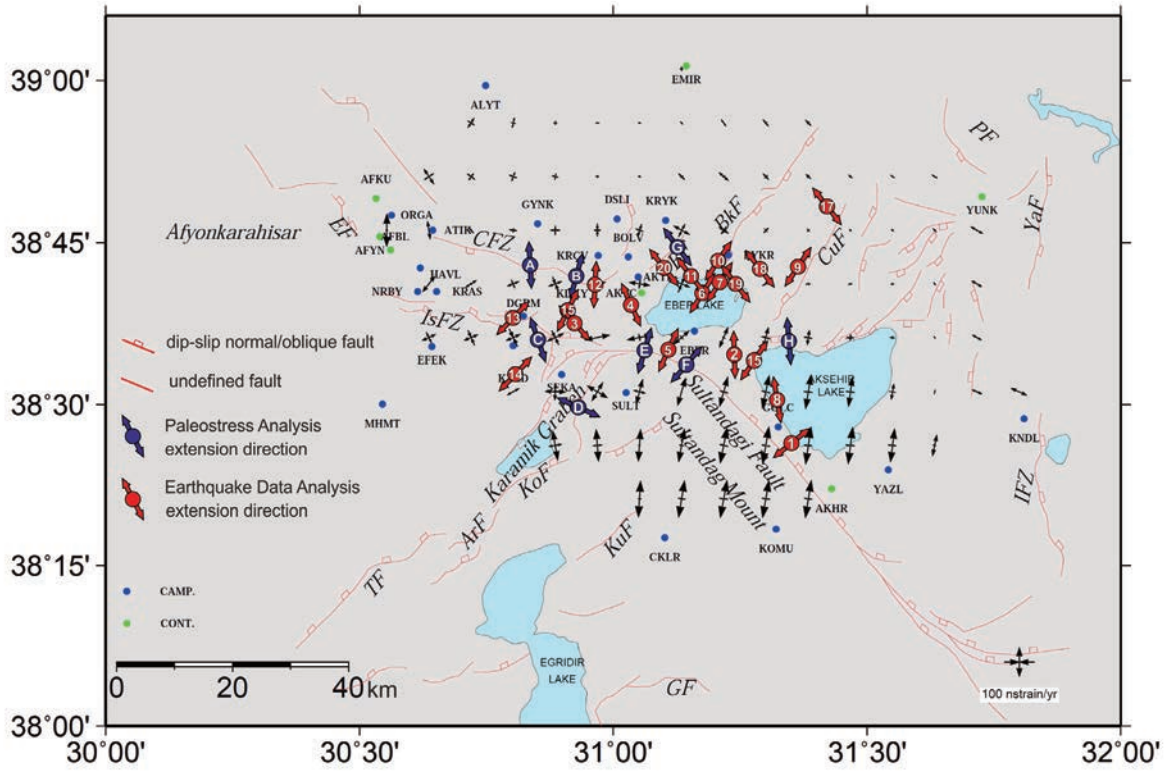

FIGURE 9. Superposed strain area based on palaeostress and earthquake data

cate a NE-SW-directed extension and a NW-SE-directed compression at a minimal level. The reason for the difference between the strain directions and the palaeostress/earthquake data is the superposing point of different tectonic blocks of the region and can be explained using the varying velocity (Figure 9, strain data).

Along the eastern part of the Işıklar and Cobanlar Fault Zone, the palaeostress analysis indicate that these normal faults have been formed under the control of a NNW-SSE to NNE-SSW extension. However, focal mechanism solutions of some recent earthquakes in this region (13,14,15 Figure 9 and Table 5) clearly testify to NE-SW-directed extensional stress which is compatible with the regional extension obtained from the GNSS analysis (Figure 9). This may be explained by clockwise rotation of the along the Sultandağı Fault. The rotation of the σ3 from NNW–SSE to NE–SW direction in this region seems to be resulted in recent activations of the western part of the Sultandağı Fault which evidenced by the 2002 Çay Earthquakes (Mw:6.0 and 6.3).

Acknowledgements. This research were financially supported by the Turkish Scientific and Technical Research Agency (TUBITAK) with the project numbered 115Y246 and Afyon Kocatepe University's projects numbered 12.TEMATIK.02. and 14.MUH.01.

REFERENCES

Acocella, V., Morvillo, P. and Funiciello, R., 2005. What controls relay ramps and transfer faults within rift zones? Insights from analogue models. Journal of Structural Geology 27, 397–408.

Aktuğ, B., Kaypak, B., Çelik, R.N., 2010. Source parameters of 03 February 2002 Çay Earthquake, Mw6.6 and aftershocks from GPS Data, Southwestern Turkey, Journal of Seismology, 14, 445-456.

Akyüz, S., Uçarkuş, G., Şatır, D., Dikbaş, A. ve Kozacı, Ö., 2006. 3 Şubat 2002 Çay depreminde meydana gelen yüzey kırığı üzerinde paleosismolojik araştırmalar. Yerbilimleri, 27 (1), 41-52.

Angelier, J., 1984.. Tectonic analysis of fault slip data sets. Journal of Geophysical Research, 89, 5835–5848.

Angelier, J., 1991. Inversion of field data in fault tectonics to obtain regional stress. III: A new rapid direct inversion method by analytical means. Geophysical Journal International, 103, 363–376.

Angelier, J., 1994. Fault slip analysis and palaeostress reconstruction. In P. L. Hancock (Ed.), Continental deformation (pp. 53–100). Oxford: Pergamon Press.

Demirtaş, R., Iravul, Y., ve Yaman M. 2002. 3 Şubat 2002 Eber ve Çay depremleri ön raporu. Jeoloji Mühendisliği Haber Bülteni, (1 - 2), 58 - 63.

Emre, Ö., Duman, T.Y., Doğan, A., Özalp, S., Tokay, F. ve Kuşcu, İ., 2003. Surface Faulting Associated with the Sultandağı Earthquake (Mw 6.5) of 3 February 2002, Southwestern Turkey. Seismological Research Letters 74 (4), 382-392.

Emre, Ö., Duman, T. Y., Özalp, S., Olgun, Ş. ve Elmacı, H., 2011. 1:250.000 scale active fault map series of Turkey, Afyon (NJ 36-5) Quadrangle. Serial number: 16, General Directorate of Mineral Research and Exploration, Ankara, Turkey.

EMSC (European-Mediterranean Seismological Centre), 2016. http://www.emsc-csem.org, 3 December 2016.

Erdik, M., Uckan, E., Sesetyan, K., Demircioğlu, M.B., Celep, U., Biro, Y., 2002. Feb.3, 2002 Sultandağı (Turkey) Earthquake. Report by the Department of Earthquake Engineering, Kandilli Obs. and Earthquake Res. Ins., Bogazici University, İstanbul, Turkey

Ergin, M., Aktar, M., Özalaybey, S., Tapirdamaz, M. C., Selvi, O., & Tarancioglu, A., 2009. A high-resolution aftershock seismicity image of the 2002 Sultandağı-Çay earthquake (Mw = 6.2), Turkey. Journal of Seismology, 13(4), 633–646. doi:10.1007/s10950-009-9155-1

Feigl, K.L., King, R.W., and Jordan, T.H., 1990. Geodetic measurements of Tectonic Deformation in the Santa Maria Fold and Thrust Belt, California. J. Geophys. Res. 9(B3), 2679–2699.

Hardcastle, K. C., & Hills, L. S., 1991. BRUTE3 and SELECT: Quick Basic 4 programmes for determination of stress tensor configurations and separation of heterogeneous populations of fault slip data. Computers & Geosciences, 17, 23–43.

Herring, T.A., King, R.W. and Mcclusky, S.C., 2010, Introduction to GAMIT/GLOBK, Release 10.4, MIT, Cambridge, MA,

GeodSuit 2017. GeodSuit User Guide, Ankara.

Gibbs, A.D., 1990. Linked faults in basin formation. Journal of Structural Geology 12, 795–803.

Kalafat, D. and Görgün, E. 2017. An example of triggered earthquakes in western Turkey: 2000–2015 Afyon-Akşehir Graben earthquake sequences,Journal of Asian Earth Sciences, 146, 103-113.

Kandilli (Boğaziçi University Kandilli Observatory And Earthquake Research Institute), 2016. http://www.koeri.boun.edu.tr/, 3 June 2016.

Koçyiğit, A., 1984. Güneybatı Türkiye ve yakın dolayında levha içi yeni tektonik gelişim. Türkiye Jeoloji Kurumu Bülteni, 27 (1), 1- 15.

Koçyiğit, A., Ünay, E. ve Saraç, G. 2000. Episodic graben formation and extensional neotectonic regime in west Central Anatolia and the Isparta Angle: a case study in the Akşehir-Afyon Graben, Turkey. Geological Society of London Special Publication, 173, 405-421.

Koçyiğit, A., Bozkurt, E., Kaymakçı, N. ve Şaroğlu, F., 2002. 3 Şubat 2002 Çay (Afyon) Depreminin Kaynağı ve Ağır Hasarın Nedenleri: Akşehir Fay Zonu, ODTÜ Tektonik Araştırma Birimi Ön Raporu, 19 s.

Koçyiğit, A. and Özacar, A. 2003. Extensional neotectonic regime through the NE edge of outer Isparta Angle, SW Turkey: new field and seismic data. Turkish Journal of Earth Sciences 12, 67–90.

Lyard F., Lefevre F., Letellier T. And Francis O., 2006, Modelling the global ocean tides: a modern insight from FES2004, Ocean Dyn., 56, 394–415.

Özden, S., Kavak, K.Ş., Koçbulut, F., Över, S. ve Temiz, H., 2002. 3 Şubat 2002 Çay (Afyon) Depremleri, Türkiye Jeoloji Bülteni, 45 (2), 49-56.

Özener, H., Dogru, A., and Acar, M., 2012, Determination Of The Displacements Along The Tuzla Fault (Aegean Region-Turkey): Preliminary Results From Gps And Precise Leveling Techniques. Journal Of Geodynamics, 1-8. Elsevier Ltd. Doi:10.1016/J.Jog.2012.06.001

Özkaymak Ç., Sözbilir, H., Tiryakioğlu, İ. ve Baybura, T., 2017. Geologic, Geomorphologic and Geodetic Analysis of Surface Deformations Observed in Bolvadin (Afyon-Akşehir Graben, Afyon). Geological bulletin of Turkey, 60, 169-188

Peacock, D.C.P., Knipe, R.J., Sanderson, D.J., 2000. Glossary of normal faults. Journal of Structural Geology 22, 291–305.

Pınar, A., 2016. Boğaziçi University Kandilli Observatory And Earthquake Research Institute Personel interview.

Shen Z.K., Jackson, D.D., Ge, B.X., 1996. Crustal deformation across and beyond the Los Angeles basin from geodetic measurements, J. Geophys. Res. 101, 27957-27980.

Tan, O., Tapırdamaz, M.C., Yörük, A., 2008. The Earthquakes Catalogues for Turkey. Turkish Journal of Earth Science, 17, 405–418.

Taymaz, T., and Tan, O., 2001. Source parameters of June 6, 2000 Orta-Çankırı (Mw ~ 6.0) and December 15, 2000 Sultandağ-Akşehir (Mw=6.0) earthquakes obtained from inversion of teleseismic P- and SH-body-waveforms. Scientific Activities 2001 Symposia - Extended Abstracts Book, pp. 96-107. Istanbul Technical University, Faculty of Mines, May 8, 2001, ATLAS DBR Press, Istanbul-Turkey, 113 pages, ISBN 975-97518-0-1.

Tiryakioğlu, İ., Baybura, T., Özkaymak, Ç., Sözbilir, H., Sandıkçıoğlu, A., Erdoğan, S., Yılmaz, İ., Uysal, M.,

Yılmaz, M., Yıldız, A., Dereli, M.A., Yalçın, M., Dumlupınar, İ., M., Yalım, H., Ertuğrul, O., 2015. Sultandağı Fayı Batı Kısmı Fay Aktivitelerinin Multidisipliner Çalışmalarla Belirlenmesi. Harita Teknolojileri Elektronik Dergisi, 7(1), 7-16.

Turan, N., 2002.Geological map of Turkey in 1:500.000 scale: Ankara sheet.Publication of Mineral Research and Explaniton Direction of Turkey (MTA), Ankara.

Turcotte, D.L., and Schubert G., 1982. Geodynamics: Applications of Continuum Physics to Geological Problems, John Wiley&Sons, New York.

Ulusay, R., Aydan, Ö., Erken, A., Tuncay, E., Kumsar, H. ve Kaya, Z., 2004. An overview of geotechnical aspects of the C ay-Eber (Turkey) earthquake. Engineering Geology 73, 51–70.

USGS, 2016. United States Geological Survey web page, http://www.usgs.gov

Yürür, T., Köse, O., Demirbağ, H., Özkaymak, Ç. ve Selçuk, L. 2003. Could the coseismic fractures of a lake ice reflect the earthquake mechanism? (Afyon earthquakes of 2 March 2002, Central Anatolia, Turkey). Geodynamica Acta 16, 83-87.

*CORRESPONDING AUTHOR: İbrahim TIRYAKIOĞLU,
Department of Geomatics, Faculty of Engineering, Afyon Kocatepe University,
Afyonkarahisar, Turkey
email: itiryakioglu@aku.edu.tr